Yb magnetic instability in $YbMn_6Ge_{6-x}Sn_x$

L. Eichenberger, D. Malterre, B. Malaman, and T. Mazet*

Institut Jean Lamour, CNRS UMR 7198, Université de Lorraine - B.P. 70239 54506 Vandœuvre-lès-Nancy, France

(Received 13 July 2017; revised manuscript received 9 August 2017; published 18 October 2017)

Yb exhibits unusual physical behavior in $YbMn_6Ge_{6-x}Sn_x$ with coexisting intermediate valent state and magnetism. We complete the (x,T) magnetic phase diagram of this system by using dc magnetization and powder neutron-diffraction experiments in a composition range ($4.60 \leqslant x \leqslant 5.30$) where the alloys were previously reported to two-phase separate. In these compounds, Mn ferromagnetically orders near room temperature while the intermediate valent Yb sublattice ($\upsilon \approx 2.8$) obeys a Doniach-like behavior. Upon increasing the $4f$ conduction electron hybridization strength through Sn for Ge substitution, the Yb magnetic moment continuously reduces as a result of the enhancement in the Kondo screening. Meanwhile the Yb magnetic ordering temperature reaches its maximum $T_{Yb} \sim 125$ K in the alloy with $x = 4.65$, before dropping upon further Sn doping. The Yb magnetic instability is located near $x \sim 5.23$, in the vicinity of which the nature of the quantum phase transition remains to be elucidated.

DOI: 10.1103/PhysRevB.96.155129

I. INTRODUCTION

Intermetallic compounds containing rare-earth elements such as Ce, Eu, or Yb exhibit a wealth of interesting physical phenomena (Kondo effect, heavy fermions, intermediate valence, unconventional superconductivity, quantum criticality, ...) which result from the immersion of their $4f$ localized magnetic moment in a conduction-electron sea [1,2]. In intermetallics, Yb may exist in a divalent $4f^{14}$ nonmagnetic state, trivalent $4f^{13}$ magnetic state, or intermediate valent state as a result of the close energetic proximity of the $4f^{13}$ and $4f^{14}$ configurations and the hybridization of the $4f$ states with the conduction electrons. The degree of hybridization, thereby the Yb valence, can be altered by control parameters such as pressure or chemical composition.

In almost all known intermediate valent Yb metallic solids, Yb is alloyed with nonmagnetic elements. In such materials (hereafter termed "standard materials"), the ground state results from the competition between the intersite Ruderman–Kittel–Kasuya–Yosida (RKKY) exchange interaction, which tends to favor magnetic order, and the local Kondo screening which tends to demagnetize the system. Doniach proposed a qualitative picture to describe the interplay between these two competing mechanisms [3].

The main result is that the ground state evolves from antiferromagnetic to nonmagnetic when the $4f$ conduction-electron exchange J is increased to a critical value J_c. Two relevant energy scales can be defined from J: the Kondo temperature $T_K \sim e^{-1/\rho J}$ and the RKKY energy $T_{AF} \sim \rho J^2$ (ρ is the density of states at the Fermi level and the quadratic dependence results from the fact that the $4f$-$4f$ coupling is mediated by the conduction electrons). For small J ($J < J_c$), corresponding to $T_K < T_{AF}$, Yb magnetically orders with usually a reduced moment with respect to the free-ion value. For $J > J_c$, the Kondo mechanism dominates leading to a nonmagnetic ground state. When $J = J_c$, the magnetic ordering temperature vanishes, which corresponds to a quantum critical point (QCP) [4]. Non-Fermi-liquid behavior and unconventional superconductivity may be observed near the QCP associated with the Yb magnetic instability [5,6].

Due to the weakness of the Yb-Yb RKKY interaction, intermediate valent Yb rarely magnetically orders and, when it does, the ordering occurs only at low temperature (<5 K) and for Yb valences close to $\upsilon \sim 3$ [7–10]. YbPd was for a long time thought to be magnetically ordered ($T_N = 1.9$ K) with strongly intermediate valent Yb ($\upsilon \sim 2.8$) [11], but it has been recently shown that YbPd contains both trivalent Yb and intermediate valent Yb ($\upsilon \sim 2.6$), coexisting in equal proportions [12], and that only trivalent Yb magnetically orders.

Our recent works on $YbMn_6Ge_{6-x}Sn_x$ ($0 \leqslant x \leqslant 6$) highlighted a new kind of intermetallics where intermediate valent Yb hybridizes with strongly polarized conduction electrons by the magnetically ordered Mn sublattice [13,14]. In these alloys, the Mn sublattice magnetically orders at or above room temperature and presents different kinds of magnetic structures (antiferromagnetic, helimagnetic, ferromagnetic) depending on composition and temperature [15,16]. While Yb is basically trivalent in $YbMn_6Ge_6$ [14], it is in an intermediate valent state in the ternary stannide $YbMn_6Sn_6$ (~2.59) [17]. The Yb valence reduces upon increasing x, most likely owing to negative chemical pressure effects due to the replacement of Ge atoms by larger Sn atoms. Yb is thus in an intermediate valent state in all pseudoternaries, the rate of change of υ with composition being larger for $x > 4.00$ (e.g., $\upsilon \sim 2.91$ for $x = 4.40$) [13,14]. These alloys exhibit astonishingly high magnetic ordering temperature of the Yb sublattice, reaching $T_{Yb} \sim 110$ K in the alloy with $x = 4.60$ [15]. In the Sn-rich part of the system, a miscibility gap, whose borders are known to depend on the annealing temperature, separates the alloys with magnetic intermediate valent Yb ($x \leqslant 4.60$) from those where Yb is nonmagnetic ($x \geqslant 5.30$) [15].

Investigations we recently performed in this composition range ($4.60 \leqslant x \leqslant 5.30$) have shown that the previously reported miscibility gap [15] closes up just above 700 °C while the alloys melt around ~800 °C. Hence, there exists a small temperature interval where the Sn-rich $YbMn_6Ge_{6-x}Sn_x$ solid solution is continuous. In this paper, we study the newly stabilized $YbMn_6Ge_{6-x}Sn_x$ alloys ($4.65 \leqslant x \leqslant 5.30$)

*thomas.mazet@univ-lorraine.fr

in powder form by using x-ray diffraction, dc magnetic measurements, and neutron-diffraction experiments. This allows us to complete the previously published (x,T) magnetic phase diagram. Section II provides the experimental details. The results are presented and discussed in Sec. III before a short conclusion in Sec. IV.

II. SYNTHESIS AND EXPERIMENTAL DETAILS

The investigated samples were annealed at 725 °C by using the procedure described in Ref. [15]. In this way, numerous new powder alloys were prepared. Their composition was verified by microprobe analysis by using a CAMECA SX 100 ($x = 4.65$, 4.95, 5.12, 5.15, 5.17, 5.20, 5.23, and 5.30). The sample purity was checked by room-temperature x-ray diffraction experiments performed using a Philips X'pert Pro diffractometer ($\lambda = 1.54056$ Å). The magnetic properties were investigated by dc magnetization measurements using a physical property measurement system (PPMS; Quantum Design) in the 5–350 K temperature range and in fields up to 9 T. The alloys have also been studied by powder neutron diffraction carried out at the Institute Laue Langevin (ILL; Grenoble, France) using the D1b two-axis diffractometer ($\lambda = 2.52$ Å) in the 2–300 K temperature range. The x-ray and neutron patterns were analyzed by Rietveld refinements using the FULLPROF software [18].

III. EXPERIMENTAL RESULTS AND DISCUSSION

A. Crystal chemistry

X-ray diffraction experiments indicate that the samples are almost single-phase with a few wt.% of the Yb_2O_3 ($T_N = 2.1$ K) [19], $MnSn_2$ ($T_N = 330$ K) [20], and $Mn_{2-x}Sn$ ($T_C \sim 250$ K) [21] impurities. As expected, the main 1-6-6 phase is isotypic with $HfFe_6Ge_6$ ($P6/mmm$) with a cell volume which expands with the Sn content. As shown in Fig. 1, it is only for $x > 5.0$ that the cell volumes depart from those expected for a fully trivalent Yb, although Yb has been found to be already in a marked intermediate valent regime ($\upsilon \sim 2.91$) within the alloy with $x = 4.40$ [13,14]. In agreement with previous findings [15], our Rietveld refinements indicated that, in these Sn-rich $YbMn_6Ge_{6-x}Sn_x$ alloys, the $2e$ and $2c$ crystallographic sites are full of Sn atoms while the $2d$ site, coplanar with the Yb site, is populated by both Ge and Sn atoms (see inset of Fig. 1).

B. Direct current magnetization and neutron diffraction

The temperature dependence of the magnetization of representative compositions is shown in Fig. 2(a). All alloys order ferromagnetically with an ordering temperature slightly decreasing upon increasing the Sn content from $T_C = 335$ K for $x = 4.65$ down to $T_C = 305$ K for $x = 5.30$. Three kinds of behavior can be distinguished upon cooling.

In the alloy with $x = 4.65$, the ferromagnetic Mn order evolves towards a low-magnetization state below ~225 K (corresponding to the $\frac{\partial M}{\partial T}$ maximum) before a rise at lower temperature due to the stabilization of the ferrimagnetic structure associated with the magnetic ordering of the Yb sublattice. This thermal dependence is very similar to that of the alloy

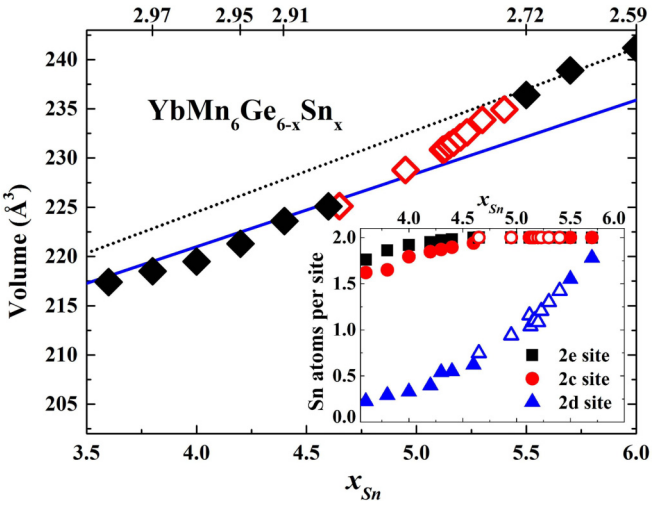

FIG. 1. Room-temperature cell volume of $YbMn_6Ge_{6-x}Sn_x$ alloys with $3.50 \leqslant x \leqslant 6.00$. The inset shows the occupancy of the metalloid sites by Sn atoms. Open symbols are for the present work; full symbols show data from Refs. [14–16]. The full oblique line marks volumes expected for a fully trivalent Yb. The dashed line corresponds to the Vegard law. Yb valence values are indicated on the top axis (data from Refs. [13,14,17]).

with $x = 4.60$ in Ref. [15], with however a higher Yb ordering temperature in the presently studied alloy ($T_{Yb} \sim 110$ K vs $T_{Yb} \sim 125$ K, taken at the low-temperature minimum of $\frac{\partial M}{\partial T}$). The neutron data at 2 K show that $x = 4.65$ indeed adopts the collinear ferrimagnetic structure where the ferromagnetic Mn and Yb sublattices are antiferromagnetically coupled with the moments pointing along the c axis. The Yb moment refines to $m_{Yb} = 0.90(8)\mu_B$, well below the free-ion value ($4\mu_B$), and lower than that of the alloy with $x = 4.60$ in Ref. [15] ($m_{Yb} = 1.13\mu_B$).

In the alloys with $4.95 \leqslant x \leqslant 5.17$, the intermediate-temperature low-magnetization state has disappeared and there is a direct transition from the ferromagnetic to the ferrimagnetic state upon cooling. This behavior has not yet been observed in the $YbMn_6Ge_{6-x}Sn_x$ series. The enlargement of the temperature extent of the ferromagnetic region upon x increasing from 4.65 to 4.95 arises from the concomitant reduction of the Yb valence, since in this family of materials lowering the valence-electron concentration promotes ferromagnetism of the Mn sublattice (see Ref. [15] and references therein). In this concentration range ($4.95 \leqslant x \leqslant 5.17$), the Yb ordering temperature (taken at the peak temperature) is found to decrease with x from $T_{Yb} \sim 110$ K in $YbMn_6Ge_{1.05}Sn_{4.95}$ down to $T_{Yb} \sim 58$ K in $YbMn_6Ge_{0.83}Sn_{5.17}$. The lack of thermal hysteresis at T_{Yb} points out the second-order nature of the transition. The richer Sn alloys ($\geqslant 5.20$) seem to behave as simple ferromagnets. We note, however, a slight increase in the magnetization of $x = 5.20$ and 5.23 below about ~70 K.

For $x = 4.95$, the analysis of the neutron thermodiffractogram indicated that the magnetic structure evolves upon cooling below T_{Yb} from a planar ferromagnetic structure towards an easy-axis ferrimagnetic structure. The spin reorientation manifests by a decrease in the intensity of the (002) diffraction peak concomitant with an increase in the intensity of the (100) peak. At 2 K, the Yb moment refines

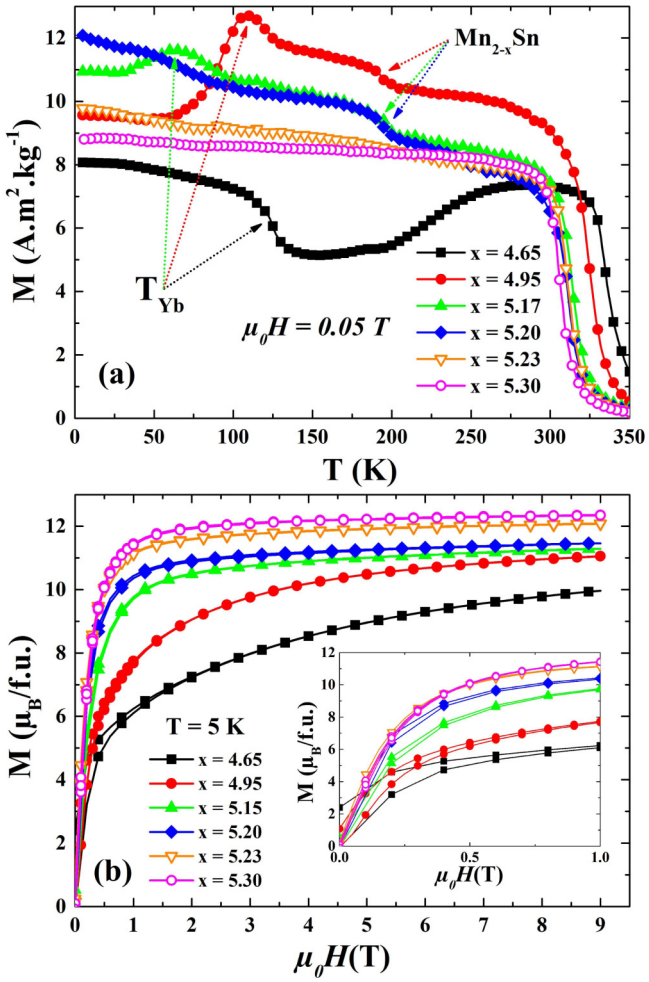

FIG. 2. (a) Thermal dependence of the magnetization of $YbMn_6Ge_{6-x}Sn_x$ ($4.65 \leqslant x \leqslant 5.30$). The little kink seen around ~200 K on some curves is due to the ferromagnetic ordering of the $Mn_{2-x}Sn$ impurity. (b) Field dependence of the magnetization at 5 K recorded on field increases and field decreases. The inset is a zoom on the low-field region.

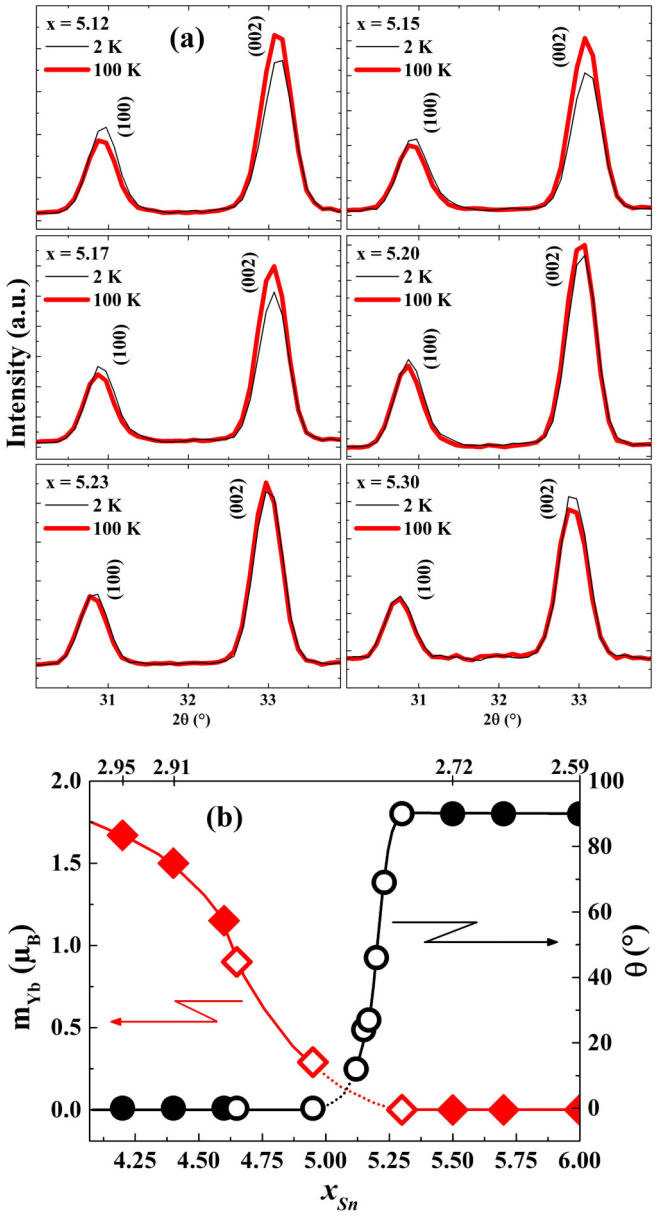

FIG. 3. (a) Selected angular region of the neutron-diffraction patterns of $YbMn_6Ge_{6-x}Sn_x$ ($x = 5.12$, 5.15, 5.17, 5.20, 5.23, and 5.30) at 100 and 2 K. (b) Composition dependence of the Yb magnetic moment m_{Yb} (left scale) and the angle θ between the c axis and the moments direction (right scale) at 2 K. Open symbols show present work; full symbols show data from Refs. [15,16]. The Yb valence values on the top axis are taken from Refs. [13,14,17]. For $5.12 \leqslant x \leqslant 5.23$, the Yb moment is likely nonzero but too low to be detected by powder neutron-diffraction experiments (see text).

to $m_{Yb} = 0.29(9)\mu_B$. A similar variation in the intensity, with a decreasing magnitude upon x increase, is also observed for the alloys with $x = 5.12$, 5.15, 5.17 [Fig. 3(a)] and even for $x = 5.20$ and 5.23, although their thermomagnetization curves [Fig. 2(a)] do not show clear evidence of Yb magnetic ordering. This indicates that a spin reorientation from the basal plane towards the c axis also takes place for $5.12 \leqslant x \leqslant 5.23$. We were, however, unable to detect a magnetic moment on Yb from our powder neutron-diffraction data. Our refinements show that the spin reorientation is not complete, the Mn moments deviating from the c axis with an angle θ increasing with x [Fig. 3(b)]. Hence, the refined magnetic structure corresponds to a collinear ferromagnetic arrangement with the Mn moments pointing between the c axis and the basal plane. However, we assume that the spin reorientation is caused by the magnetic ordering of Yb, whose magnetic moment is too low to be detected by powder neutron diffraction and that, consequently, these alloys are actually ferrimagnetic at 2 K.

Finally, for $x = 5.30$ the intensity of the (002) Bragg peak grows continuously upon cooling: This alloy is an easy-plane ferromagnet with the sole Mn sublattice ordered and no magnetic ordering of Yb, as the Sn-rich $YbMn_6Ge_{6-x}Sn_x$ alloys of Refs. [15,16].

Throughout the investigated Sn concentration range, the Mn moment m_{Mn} keeps its usual magnitude in RMn_6Sn_6 close to $\sim 2.2\mu_B$. The maximum low-temperature magnetization [Fig. 2(b)] thus reaches $12.5\mu_B$/f.u. in the simple ferromagnet $x = 5.30$ alloy. The maximum magnetization decreases upon reducing the Sn content due to the increasing magnitude of

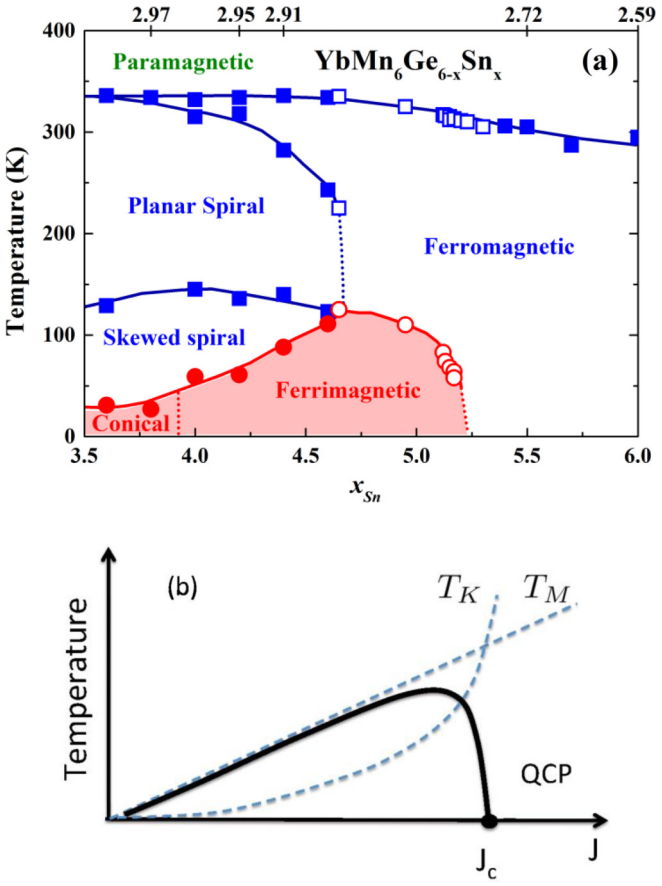

FIG. 4. (a) The (x,T) magnetic phase diagram of $YbMn_6Ge_{6-x}Sn_x$ $(3.5 \leqslant x \leqslant 6)$. Squares show Mn magnetic transitions; circles show Yb magnetic ordering. The data in full symbols as well as the Yb valence values on the top axis are taken from Refs. [13–17]. The data in open symbols are from the present thermomagnetization experiments. For a detailed description of the various magnetic structures, see Ref. [15]. (b) Schematic Doniach-like diagram with a linear dependence in J of the characteristic temperature T_M of the Mn-Yb exchange interaction.

the Yb moment [Fig. 3(b)] which couples antiferromagnetically with the Mn moments. This reduction in the maximal magnetization is accompanied by a *hardening* of the magnetic behavior; that is, the saturation is reached at higher fields and weak irreversibilities appear at low field. This as well as the spin reorientation induced by the Yb magnetic ordering suggests that the Yb moment keeps an orbital contribution even when it is strongly Kondo screened.

C. (x,T) magnetic phase diagram

The data we collected allow us to complete the (x,T) phase diagram presented in Ref. [15] [Fig. 4(a)]. In the $3.5 \leqslant x \leqslant 6$ concentration range, the low-temperature part bears strong qualitative similarities with the well-known Doniach diagram described above [3]. This diagram has been reproduced experimentally in several standard Yb or Ce materials [1,2,22,23]. However, the Doniach picture cannot be used as is because, in rare-earth transition-metal intermetallics such as $YbMn_6Ge_{6-x}Sn_x$, the Kondo screening competes with the Mn-Yb exchange interaction which largely dominates the much weaker Yb-Yb interaction [24,25]. In addition, theoretical works indicate that the exchange field at the Yb site has a much stronger effect in the intermediate valence regime [26]. As a result, the Yb magnetic ordering temperatures in $YbMn_6Ge_{6-x}Sn_x$ are one or two order(s) of magnitude higher than those of the scarce standard materials where intermediate valent Yb magnetically orders.

Nevertheless, we believe that the Doniach picture could be modified to capture the Yb behavior within $YbMn_6Ge_{6-x}Sn_x$ $(3.5 \leqslant x \leqslant 6)$. The Mn-Yb interaction arises from the local hybridization of the $4f$ states of Yb with the $5d$ conduction electrons which are strongly polarized due to their spin-dependent covalent interaction with the self-polarized $3d$ states of neighboring Mn atoms [27]. Therefore, the characteristic temperature of the magnetic coupling between Yb and Mn moments should be linearly dependent in J ($T_M \sim \rho J$) instead of the quadratic dependence of the RKKY interaction prevailing in standard materials. The resulting diagram is sketched in Fig. 4(b). It qualitatively reproduces the experimental phase diagram.

In $YbMn_6Ge_{6-x}Sn_x$, the control parameter which allows increasing J (i.e., reducing the Yb valence) is the chemical pressure reduction owing to the replacement of Ge by larger Sn. For low Sn content, J is small and, because $T_M > T_K$, Yb orders but with a low ordering temperature. Upon increasing x, J increases, then the magnetic ordering of Yb first increases up to $T_{Yb} = 125$ K for $x = 4.65$, then decreases strongly until the Yb magnetic ordering is lost for $x > 5.23$. Concomitantly, the Yb moment continuously reduces due to growing Kondo screening. Above the critical value J_c corresponding to $x = 5.23$, the Kondo energy dominates $T_K > T_M$.

The strong Mn-Yb exchange interaction enables the stabilization of magnetically ordered Yb up to a high degree of hybridization (i.e., for low Yb valence) compared with the standard materials. Assuming the Yb valence changes linearly with x between $x = 4.40$ $(\upsilon = 2.91)$ and $x = 5.50$ $(\upsilon = 2.72)$, we estimate that the Yb valence is $\upsilon \sim 2.75$ for $x = 5.23$, the richest Sn alloy within which the magnetism of Yb is found to survive. In standard intermediate valent Yb materials, the Yb magnetic instability happens for υ closer to $\sim$3 and involves generally an antiferromagnetic Yb sublattice [2,6]. In the latter, quantum criticality is often observed in the vicinity of the Yb magnetic instability. In $YbMn_6Ge_{6-x}Sn_x$, a still-unexplored situation that is potentially rich in new phenomena to explore occurs: the 0 K quantum phase transition concerns a ferromagnetic Yb antiferromagnetically coupled with a ferromagnetic Mn sublattice. The transition at T_{Yb} far above 0 K is continuous (second order). In metallic systems with a nonvanishing homogeneous magnetization, the transition often evolves from second order to first order upon cooling close to 0 K [28]. On the other hand, quenched disorder, as in the metalloid $2d$ site of $YbMn_6Ge_{6-x}Sn_x$ (see inset of Fig. 1), favors continuous transitions [28].

IV. CONCLUSION

We have completed the Sn-rich part of the previously published (x,T) magnetic phase diagram of the $YbMn_6Ge_{6-x}Sn_x$ system. Upon increasing x (i.e., upon increasing the $4f$

conduction-electron hybridization), the Yb sublattice behaves in a Doniach-like manner: its magnetic ordering goes to a maximum for $x = 4.65$ before falling off rapidly until the Yb long-range magnetic order disappears for $x > 5.23$. Due to the strong Mn-Yb exchange interactions, the Yb ordering temperature is unusually high (up to $T_{Yb} \sim 125$ K) while the Yb magnetic instability is shifted towards strongly intermediate valent Yb (roughly $\upsilon \sim 2.75$) compared with materials where Yb is mixed with nonmagnetic elements. Further investigations at very low temperature in the vicinity of the Yb magnetic instability are necessary to probe the nature of the ensuing quantum singularities. That would provide a better understanding of the interplay between the charge and spin degrees of freedom in strongly correlated electron materials.

ACKNOWLEDGMENTS

We are indebted to the Institut Laue-Langevin (Grenoble, France) for the provision of research facilities (Expt. No. 5-31-2402). We are grateful to R. Esmilaire and H. Charaf for their participation in finding the borders of the miscibility gap.

[1] For a review, see P. Coleman in *Handbook of Magnetism and Advanced Magnetic Materials*, edited by H. Kronmüller and S. Parkin (Wiley, New York, 2007), and references therein.
[2] J. Flouquet and H. Harima, arXiv:0910.3110.
[3] S. Doniach, Physica B + C (Amsterdam) **91**, 231 (1977).
[4] P. Coleman and A. Schofield, Nature (London) **433**, 226 (2005).
[5] H. V. Löhneysen, A. Rosch, M. Vojta, and P. Wölfe, Rev. Mod. Phys. **79**, 1015 (2007).
[6] P. Gegenwart, Q. Si, and F. Steglich, Nat. Phys. **4**, 186 (2008).
[7] E. D. Mun, S. L. Budko, C. Martin, H. Kim, M. A. Tanatar, J.-H. Park, T. Murphy, G. M. Schmiedeshoff, N. Dilley, R. Prozorov, and P. C. Canfield, Phys. Rev. B **87**, 075120 (2013).
[8] E. Bauer, R. Hauser, L. Keller, P. Fischer, O. Trovarelli, J. G. Sereni, J. J. Rieger, and G. R. Stewart, Phys. Rev. B **56**, 711 (1997).
[9] C. Klingner, C. Krellner, M. Brando, C. Geibel, F. Steglich, D. V. Vyalikh, K. Kummer, S. Danzenbächer, S. L. Molodtsov, C. Laubschat, T. Kinoshita, Y. Kato, and T. Muro, Phys. Rev. B **83**, 144405 (2011).
[10] H. Nakai *et al.*, J. Phys. Soc. Jpn. **82**, 124712 (2013).
[11] P. Bonville, J. Hammann, J. A. Hodges, P. Imbert, and G. J. Jéhanno, Phys. Rev. Lett. **57**, 2733 (1986).
[12] R. Takahashi, T. Honda, A. Miyake, T. Kagayama, K. Shimizu, T. Ebihara, T. Kimura, and Y. Wakabayashi, Phys. Rev. B **88**, 054109 (2013).
[13] T. Mazet, D. Malterre, M. François, C. Dallera, M. Grioni, and G. Monaco, Phys. Rev. Lett. **111**, 096402 (2013).
[14] T. Mazet, D. Malterre, M. François, L. Eichenberger, M. Grioni, C. Dallera, and G. Monaco, Phys. Rev. B **92**, 075105 (2015).
[15] T. Mazet, H. Ihou-Mouko, D. H. Ryan, C. J. Voyer, J. M. Cadogan, and B. Malaman, J. Phys.: Condens. Matter **22**, 116005 (2010).
[16] T. Mazet, R. Welter, and B. Malaman, J. Magn. Magn. Mater. **204**, 11 (1999).
[17] L. Eichenberger, G. Venturini, B. Malaman, L. Nataf, F. Baudelet, and T. Mazet, J. Alloys Compd. **695**, 286 (2017).
[18] J. Rodriguez-Carvajal, Phys. B (Amsterdam, Neth.) **192**, 55 (1993).
[19] R. M. Moon, W. C. Koelher, H. R. Child, and R. J. Raubenheimer, Phys. Rev. **176**, 722 (1968).
[20] J. S. Kouvel and C. C. Hartelius, Phys. Rev. **123**, 124 (1961).
[21] J. H. Xu, X. M. Liu, Y. H. Xia, W. Y. Yang, H. L. Du, J. B. Yang, Y. Zhang, and Y. C. Yang, J. Appl. Phys. **113**, 17A921 (2013).
[22] A. L. Cornelius, J. S. Schilling, D. Mandrus, and J. D. Thompson, Phys. Rev. B **52**, R15699(R) (1995).
[23] B. Chevalier, A. Wattiaux, and J.-L. Bobet, J. Phys.: Condens. Matter **18**, 1743 (2006).
[24] M. S. S. Brooks, L. Nordström, and B. Johansson, J. Phys.: Condens. Matter **3**, 2357 (1991).
[25] P. Tils, M. Loewenhaupt, K. H. J. Buschow, and R. S. Eccleston, J. Magn. Magn. Mater. **210**, 196 (2000).
[26] J. L. Ferreira, S. Burdin, and C. Lacroix, J. Science: Adv. Mater. Devices **1**, 164 (2016).
[27] A. R. Williams, R. Zeller, V. L. Moruzzi, C. D. Gellat, and J. Kubler, J. Appl. Phys. **52**, 2067 (1981).
[28] M. Brando, D. Belitz, F. M. Grosche, and T. R. Kirkpatrick, Rev. Mod. Phys. **88**, 025006 (2016).